Advanced Materials Interfaces

ADVANCED MATERIALS INTERFACES Open Access

www.advmatinterfaces.de

RESEARCH ARTICLE OPEN ACCESS

High Quality MoS_2 Layered Thin Films Obtained by Ionized Jet Deposition Investigated by X-ray Absorption Spectroscopy at S $L_{2,3}$ and Mo $M_{2,3}$ Edges

Giulia Giovanelli[1] | Alessandro Lodi[1] | Angelo Giglia[2] | Nicola Mahne[2] | Rahul Kesarwani[3] | Jana Vejpravova[3] | Steffen Rühl[4,5] | Giovanni Ligorio[4,5] | Emil J. W. List-Kratochvil[4,5] | Lucia Nasi[6] | Melanie Timpel[7] | Marco V. Nardi[7] | Luca Pasquali[1,2,8]

[1]Department of Engineering "Enzo Ferrari", University of Modena and Reggio Emilia, Modena, Italy | [2]CNR – Istituto Officina Dei Materiali (IOM), Trieste, Italy | [3]Department of Condensed Matter Physics, Faculty of Mathematics and Physics, Charles University, Prague, Czech Republic | [4]Department of Physics, Department of Chemistry & Center for the Science of Materials Berlin, Humboldt-Universität zu Berlin, Berlin, Germany | [5]Helmholtz–Zentrum Berlin für Materialien Und Energie, Berlin, Germany | [6]IMEM-CNR, Institute of Materials for Electronics and Magnetism, Parma, Italy | [7]CNR-IMEM Institute of Materials for Electronics and Magnetism, Trento unit c/o Fondazione Bruno Kessler, Trento, Italy | [8]Department of Physics, University of Johannesburg, Johannesburg, South Africa

Correspondence: Marco V. Nardi (marcovittorio.nardi@cnr.it) | Luca Pasquali (luca.pasquali@unimore.it)

Received: 4 March 2026 | **Revised:** 25 June 2026 | **Accepted:** 8 July 2026

Keywords: ionized jet deposition | molybdenum disulfide | x-ray absorption spectroscopy

ABSTRACT

We present a comparative soft x-ray absorption spectroscopy (XAS) study of the sulfur $L_{2,3}$ and molybdenum $M_{2,3}$ absorption edges in MoS_2 prepared by different fabrication routes, including bulk crystallization, mechanical exfoliation, chemical vapor deposition (CVD), and ionized jet deposition (IJD). The S $L_{2,3}$ edges reveal pronounced differences in pre-edge and main-edge fine structure that sensitively reflect the degree of structural order, dimensionality, and electronic hybridization between S 3p and Mo 4d states. Bulk, exfoliated, and CVD-grown samples exhibit well-resolved multiple features characteristic of layered and ordered two-dimensional (2D) MoS_2, whereas as-deposited IJD-grown films display broadened, weakly structured spectra consistent with an amorphous phase and poorly defined stoichiometry. Upon moderate annealing at 250°C, IJD-grown films develop clear spectral signatures of layered MoS_2, indicating the formation of an ordered crystalline 2H-MoS_2 phase. Complementary analysis of the Mo $M_{2,3}$ edges shows a concomitant narrowing and energy shift of the M_3 feature toward values typical of well-ordered 2D MoS_2. These results demonstrate that S $L_{2,3}$ and Mo $M_{2,3}$ XAS provide a sensitive probe of synthesis-dependent electronic structure in MoS_2 and confirm IJD as a viable, low-temperature route to electronically ordered 2D MoS_2 phases.

1 | Introduction

Two-dimensional (2D) transition metal dichalcogenides (TMDCs) have emerged as a versatile class of materials for applications spanning electronics, optoelectronics, energy conversion, and sensing, owing to their layered structure and tunable electronic properties. Among them, molybdenum disulfide (MoS_2) is certainly considered the archetypal example in the class [1–5]. Beyond its favorable band structure, MoS_2 combines chemical stability with a rich electronic configuration arising from the hybridization between Mo 4d and S 3p states. This makes it a promising material for a wide range of applications, including 2D (opto)electronic devices, electrocatalysis for hydrogen evolution and water splitting [6, 7], as well as emerging

biomedical uses such as photothermal therapy and bone tissue engineering [8, 9]. The functional performance of MoS_2, however, is highly sensitive to stoichiometry, defect density, crystallinity, and interlayer coupling, all of which are strongly influenced by the synthesis method.

To date, both top-down and bottom-up approaches have been explored for the fabrication of MoS_2 films. Mechanical and liquid-phase exfoliation techniques can yield high-quality flakes with minimal defect density, but they suffer from limited lateral dimensions, poor reproducibility, and intrinsic scalability constraints [10, 11]. Bottom-up methods, including chemical vapor deposition (CVD) [12–14], thermal decomposition of Mo-based precursors [15, 16], sol–gel-derived processes [17, 18], and physical vapor deposition (PVD) techniques such as pulsed laser deposition and magnetron sputtering [19–24], offer improved control over film thickness and coverage. Nevertheless, many of these approaches still face challenges related to large-area uniformity, process complexity, substrate compatibility, and reproducibility of key electronic properties.

Recently, ionized jet deposition (IJD) has been proposed as a competitive and industrially scalable technique for the growth of MoS_2 thin films [25–27]. IJD is a pulsed electron-based deposition method that enables the transfer of material from a target to the substrate while preserving chemical composition and enabling growth at relatively low substrate temperatures [27–33].

In this context, it is intriguing to elucidate how the different fabrication methods can influence the electronic properties. Photoelectron spectroscopy, either with x-rays or UV photons, is widely applied, as it probes the evolution of the filled electronic states: the valence band and the core levels, providing rich information on chemical bonding, reactivity, stoichiometry, and electronic band structure. X-ray absorption spectroscopy (XAS), on the other hand, provides complementary element-specific sensitivity to unoccupied electronic states and local coordination [34]. In particular, the sulfur $L_{2,3}$ and molybdenum $M_{2,3}$ absorption edges directly probe the S 3p–Mo 4d hybridized states that govern the electronic and optical properties of MoS_2 [35–38]. Subtle variations in the XAS lineshape can reveal changes in defect states, oxidation, and interlayer coupling, which are often inaccessible by conventional structural probes alone. In particular, XAS has been demonstrated as a uniquely powerful probe of local electronic structure in amorphous systems and 2D amorphous/crystalline hybrid materials, where long-range order is absent and conventional diffraction probes yield limited information [39, 40]. The synthesis of 2D amorphous and crystalline phase composites from metal-based systems has attracted growing interest as a route to combining the mechanical robustness of bulk materials with the functional properties of 2D phases [41–43], and IJD-grown MoS_2 films after annealing represent a compelling example of such a composite architecture.

In this work, we present a comparative XAS study of the S $L_{2,3}$ and Mo $M_{2,3}$ absorption edges in a series of MoS_2 samples prepared by mechanical exfoliation, CVD, bulk crystallization, and IJD. By systematically analyzing differences in edge position, spectral weight distribution, and fine structure features, we aim to elucidate the influence of synthesis conditions on the local electronic structure of MoS_2. Emphasis is placed on IJD-grown films, which not only enable detailed investigation of the structural characteristics of MoS_2 and their relation to dimensionality, bonding, and electronic properties but also represent an upscalable, cost-effective, and environmentally friendly deposition technique.

2 | Results and Discussion

XAS spectra taken in correspondence with the S $L_{2,3}$ absorption edges for the different samples are compared in Figure 1. All spectra are characterized by a pronounced absorption feature above a photon energy of 170 eV, associated with the main absorption edge and arising from optical transitions from spin-orbit split S $2p_{3/2}$ (L_3) and $2p_{1/2}$ (L_2) states into empty S 3d states hybridized with Mo 5p states [36, 37]. In addition, a well-defined pre-edge structure is observed below 169 eV, which is related to less-favored (due to dipole selection rules) optical transitions from S $2p_{3/2}$ – $2p_{1/2}$ levels to hybridized S 3p—Mo 4d empty states [37].

The three topmost curves in Figure 1 refer to bulk, ultrathin exfoliated, and CVD-grown films, respectively. The lineshape is similar, revealing a complex fine structure, with features that have been labelled *a*–*e* (for the pre-edge) and *f*–*i* (for the main edge), in agreement with the assignment of Ref [37]. In particular, the pre-edge regions, which are very sensitive to the electronic configuration [36–38], are shown in greater detail in Figure 2a, while in Figure 2b a representative fit of the spectrum recorded on the bulk MoS_2 is reported, as obtained by a superposition of multiple Voigt peaks. The two spectral envelopes in dark and light gray reflect the spin-orbit split transitions from $2p_{3/2}$ (L_3) and $2p_{1/2}$ (L_2) initial states to the same final states: they are replicas shifted by 1.2 eV, i.e., the spin-orbit splitting between $2p_{3/2}$ and $2p_{1/2}$ in sulfur, with a branching intensity ratio of 1/2 between the two. The peaks corresponding to the L_3 pre-edge are labelled following the convention of Ref [37].

In Figure 2b, the decomposition of the pre-edge region is shown representatively only for the bulk sample. The CVD-grown and exfoliated MoS_2 samples clearly show the same spectral features. However, it can be noticed that for these films, the features are even more resolved with respect to the bulk. The richness of the edge and pre-edge regions is closely related to the typical electronic structure of layered and ordered MoS_2. Based on the calculations shown and discussed in Ref [37], it can be speculated that the higher definition of features *a*–*e* in the CVD-grown and exfoliated samples reflects the 2D nature of these films. Interestingly, defect-related states at photon energies below feature *a* previously associated with a high density of corrugations at the edges of MoS_2 sheets [37] are not observed in any of the investigated samples. A high density of sulfur vacancies is also excluded, since likewise this would induce absorption features at lower photon energies with respect to feature *a*, due to the development of electronic states in the main gap of MoS_2 [44].

Concerning the IJD samples, the spectra of as-deposited thin and thick films are similar to those of MoS_2 films obtained via sputtering [38]. Both edge and pre-edge features (Figures 1 and 2) do not show a well-resolved fine structure. This is consistent with films that mostly present an amorphous nature with a poorly defined stoichiometry. More specifically, the as-

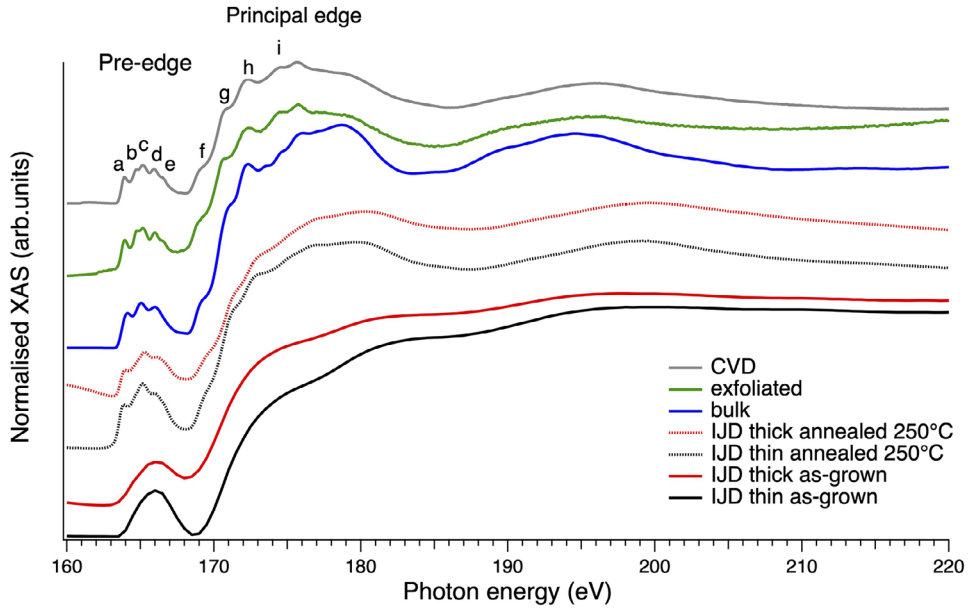

FIGURE 1 | S $L_{2,3}$ edges of the different MoS_2 samples, as indicated in the figure.

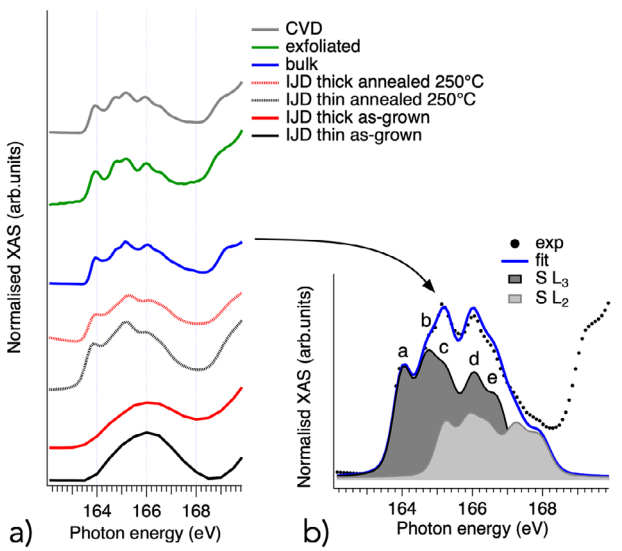

FIGURE 2 | (a) Pre-edge S $L_{2,3}$ spectra of the different MoS_2 samples, as indicated in the figure; (b) Representative fit of the spectrum of bulk MoS_2.

deposited IJD films consist of amorphous, sulfur-enriched Mo_xS_y nanoclusters with a S/Mo atomic ratio of approximately 2.5 (as determined by x-ray photoelectron spectroscopy - XPS - in Ref [33]) and a high concentration of defects, dangling bonds, and multiple sulfur chemical environments including Mo–S–S–Mo, Mo–Mo–S, and elemental S species. This atomic disorder is directly responsible for the absence of the well-resolved XAS fine structure observed in the ordered reference samples (bulk, CVD, exfoliated), which arises from long-range-ordered S 3p–Mo 4d hybridization in the 2H-MoS_2 phase. The behavior is analogous to that of magnetron-sputtered MoS_2 films in the as-deposited state [38]. Upon annealing at a moderate temperature of 250°C, the lineshape strongly changes for both thin and thick IJD-MoS_2 films, with an overall shift to lower photon energies and the development of fine structures that tend toward those typical of layered MoS_2. Annealing induces a partial reorganization of the amorphous nanoclusters into crystalline 2H-MoS_2 nanosheets (predominantly 1–4 layers) embedded within a residual amorphous MoS_2 matrix (see Figure 3 and Refs [25, 33]). This dual-phase composite structure — crystalline nanosheets encapsulated in an amorphous matrix — distinguishes the annealed IJD films from the single-phase reference samples and accounts for the intermediate XAS lineshape observed after annealing: well-resolved features characteristic of 2D MoS_2 emerge but with reduced contrast relative to the purely crystalline references. It is noteworthy that the retention of the amorphous matrix can be favorable: it provides mechanical encapsulation and passivation of the crystalline nanosheets, suppressing environmental doping and preserving their 2D electronic properties over time [33].

We stress that the development of this 'intermediate' lineshape type has been observed also previously upon annealing of sputtered films [38], but at much higher annealing temperatures of about 900°C. The choice of 250°C as the post-deposition annealing temperature is motivated here by two complementary criteria. From a technological standpoint, 250°C is compatible with a broad range of substrates relevant for flexible and wearable electronics, including high-performance polymers such as polyimide (glass transition temperature typically above 300°C), making IJD uniquely suited for device integration on flexible supports where conventional CVD or PLD crystallization temperatures (700°C–900°C) are incompatible. From a materials perspective, 250°C represents the minimum temperature at which significant structural reorganization of the amorphous Mo_xS_y nanoclusters into 2H-MoS_2 nanosheets occurs, while deliberately retaining the amorphous MoS_2 encapsulation matrix. The higher kinetic energy of species in the IJD plasma plume, compared to conventional sputtering, lowers the activation energy for the amorphous-to-crystalline transition and is responsible for the markedly lower crystallization temperature of IJD vs. sputtered MoS_2

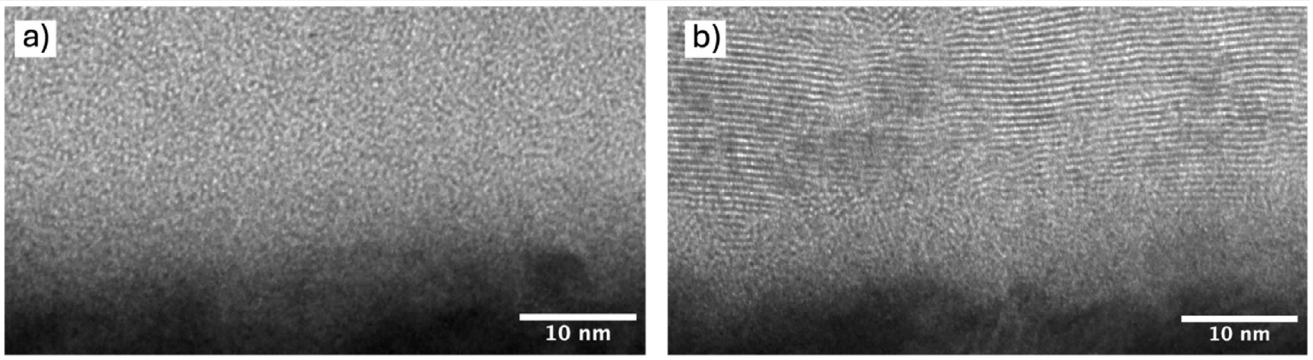

FIGURE 3 | Bright field TEM images of the (a) as-deposited and (b) annealed IJD-MoS_2 thick film. TEM lamellae were prepared by FIB lift-out; bright-field imaging was performed at 200 kV using a field-emission JEOL JEM-2200FS equipped with an in-column Omega energy filter.

films [25, 33]. Furthermore, XRD measurements on comparable IJD-MoS_2 films (Ref [33]) confirm the absence of diffraction peaks in the as-deposited state and the appearance of the hexagonal 2H-MoS_2 (002) reflection at $2\theta \approx 14.4°$ (interlayer spacing 6.19 Å, in excellent agreement with the standard value of 6.14 Å) after annealing at 250°C, fully consistent with the XAS results presented here. XPS, utraviolet photomeission (UPS), and electron energy loss spectroscopy (EELS) characterization reported in Ref [33] further confirm the chemical composition, stoichiometric S/Mo ≈ 2, and semiconducting properties of the annealed IJD films. Figure 3 displays bright-field transmission electron microscopy (TEM) images of the IJD-MoS_2 thick film in the (a) as-deposited and (b) annealed states, confirming the transition from amorphous MoS_2 in the as-deposited film to crystalline, layered MoS_2 after annealing at 250°C, as previously reported [25, 33]. This is intriguing, since it confirms that already at moderate annealing temperatures, compatible with most fabrication methods, even involving growth on polymeric substrates, MoS_2 films produced by IJD start to present characteristics that are typical of layered MoS_2 [33].

In Figure 4a,b, the $M_{2,3}$ edges of Mo in the different samples are compared. The $M_{2,3}$ edges are associated with the optical transmission from Mo $3p_{1/2}$ (M_2) and $3p_{3/2}$ (M_3) to unoccupied Mo 4d orbitals, which characterize the bottom of the conduction band. The differences are less pronounced with respect to the S $L_{2,3}$ edge spectra. These can be recognized better in Figure 4b, where only the M_3 edge is shown. As reported in Table 1, the centroid of the peak tends to shift from 396.7 eV for the as-deposited IJD films toward lower photon energies for the other samples. After annealing, the IJD peaks shift by 0.2 eV to lower energies for both thin and thick films; then it reaches the values of 369.3 eV for bulk and CVD-grown films and 396.1 eV for the exfoliated film. In parallel, the full width at half maximum (FWHM) of the structure reduces sizably when comparing IJD films and well-organized 2D MoS_2 samples, i.e., bulk, CVD-grown, and exfoliated ones.

As noted in Ref [36] in the discussion of the Mo $L_{2,3}$ edges, transitions into Mo 4d final states exhibit a slight linear dichroism, i.e., transitions occurring in-plane (with respect to the 2D MoS_2 basal plane) appear at slightly lower energies than those involving states oriented parallel to the *c* axis of MoS_2. In the same way, the M_3 edge can be considered as a superposition of two slightly shifted contributions, with the lower-energy component corresponding to in-plane transitions and the higher-energy component to out-of-plane transitions. In our experimental setup (s-polarization), the electric field of the incoming radiation is always parallel to the sample plane, which coincides with the basal plane of 2D MoS_2 for bulk, CVD-grown, and exfoliated samples. This favors in-plane optical transitions, corresponding to lower absorption photon energies. On the other hand, the lack of structural order in as-deposited IJD samples makes the two transitions equally probable. Besides this, the anisotropic configuration of Mo 4d empty states typical of layered MoS_2 [36] is not established for the as-deposited films [33]. This leads to an overall broadening of the entire structure and a shift of the centroid toward higher photon energies. Annealed IJD-MoS_2 films represent an intermediate step, due to the formation of ordered layered MoS_2 nanosheets that are mostly oriented parallel to the film plane. The narrower M_3 peak shown by the annealed IJD-MoS_2 thin film with respect to the annealed thick one seems to indicate a higher degree of order: in the thin film, the density of layered MoS_2 nanosheets lying parallel to the substrate plane appears to be higher. This is also reflected by the S $L_{2,3}$ edges in Figure 2a, where the fine structure typical of the 2D phase of MoS_2 is more defined in the annealed thin film with respect to the annealed thick film.

3 | Conclusions

X-ray absorption spectroscopy in the soft x-rays is a valuable technique to probe the complexity of the empty states and the evolution of the conduction band in transition metal dichalcogenides. This is applied in the present work to MoS_2 thin films produced by different methods. Thin films fabricated by ionized jet deposition (IJD), a technique applied only recently for the synthesis of thin films of these materials, but which promises a high throughput at moderate costs, are compared to prototypical examples of highly ordered MoS_2 systems: a bulk crystal, a CVD-grown film, and a mechanically exfoliated film. S $L_{2,3}$ and Mo $M_{2,3}$ edges show a rich fine structure that is correlated to the film quality. While as-deposited IJD-MoS_2 films do not show structures associated to the formation of layered 2D MoS_2, coherently with a generally amorphous layer of poorly defined stoichiometry, already after a moderate annealing temperature of 250°C, the evolution of the spectral lineshape of both edges reveals the presence of an ordered 2D phase related to the

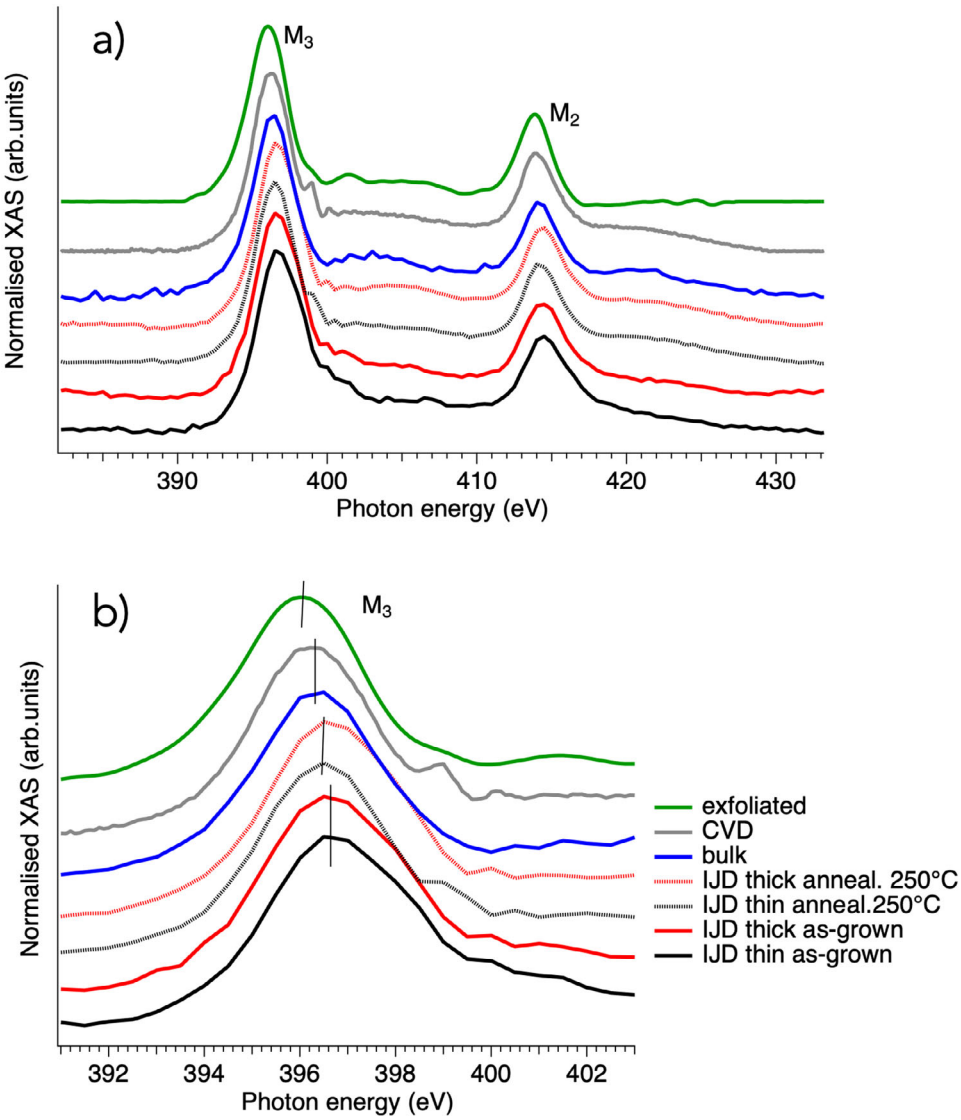

FIGURE 4 | (a) Mo $M_{2,3}$ edges and (b) detail of the Mo M_3 edge spectra of the different MoS_2 samples, as indicated in the figure.

TABLE 1 | Energy position of M_3 peak and FWHM for the different MoS_2 samples.

Sample	Peak position ± 0.1(eV)	FWHM ± 0.1(eV)
IJD thin—as deposited	396.7	3.3
IJD thick—as deposited	396.7	3.3
IJD thin—annealed	396.5	3.1
IJD thick—annealed	396.5	3.3
Bulk	396.3	3.0
CVD	396.3	2.9
Exfoliated	396.1	3.0

formation of domains of ordered and stacked layers preferentially aligned parallel to the substrate plane and possessing the full characteristics of 2H-MoS_2 in terms of electronic structure and empty states configuration. It is noteworthy that other conventional production methods, such as sputtering, do not reveal analogous features until much higher annealing temperatures of the films are reached.

4 | Experimental Section

MoS_2 single-crystal bulk samples synthesized by flux zone growth from 2D Semiconductors were used as received, after fresh cleavage by 'blue' adhesive tape (Nitto Denko ELP BT-150P-LC) just before insertion into the UHV vessel for spectroscopy measurements.

CVD-grown MoS_2 monolayers were synthesized on Si/SiO_2 substrates with a 300- nm thick thermally grown oxide layer.

The substrate was cleaned through subsequent sonication in acetone and isopropanol (Sigma–Aldrich). The fabrication of MoS_2 took place in a quartz tube using a horizontal furnace with two heating zones, under atmospheric pressure, employing argon as the carrier gas. Initially, the tube was connected to an argon gas line at one end and to a bubbler filled with a 100 mM aqueous solution of KOH. The tube was flushed with argon at a continuous flow of 200 cm^3 min^{-1} at a temperature of ~25°C for 15 min. The precursor, MoO_2 (30 mg) powder (Sigma–Aldrich: LOT: STBH3472, purity 99%), was placed in the crucible at the first heating zone (high temperature), and the substrate was placed face-down on top of the crucible. Simultaneously, 100 mg of sulfur (Thermo Scientific LOT: T29G013, purity 99.9995%) was placed in a tube, 20 cm away, at the second heating zone (low temperature). Maintaining a constant argon flow rate of 120 cm^3 min^{-1}, the temperature was subsequently increased in the tube at a constant rate of 40°C min^{-1}. When the temperature reached ~670°C in the first heating zone, the heating in the second zone was initiated. The temperatures were held constant at ~820°C in the first zone and ~180°C in the second zone for 10 min, after which the furnace was opened, and the system was allowed to cool to ambient temperature.

Exfoliation of MoS_2 monolayers was achieved by a gold-mediated template strip approach described in detail elsewhere [45, 46]. Gold was evaporated (100 nm, 0.5 nm/s) onto a clean 10 cm native oxide silicon wafer (Siegert Wafer, <100>, 525 µm thickness), followed by a thicker layer of copper (600 nm, 2 nm/s) to facilitate a higher etch rate. After evaporation, cleaned glass slides (1.5 × 1 cm) were glued onto the surface with the help of a UV-curable epoxy (Ossila E132 encapsulation epoxy). After the epoxy cured, the glass slides were stripped off the surface to reveal a fresh, clean, and smooth gold surface. With the help of Kapton tape, a MoS_2 single crystal (2D semiconductors, synthetic bulk crystal) was cleaved to reveal a fresh crystal face, which then was swiftly pressed onto the gold. The whole stack was then placed onto a hotplate. After heating for 2 min at 200°C, the substrates were removed, and the MoS_2-carrying Kapton was carefully peeled off, revealing MoS_2 mono- and multilayers. For transfer, a solution of polystyrene in toluene (90 mg/ml) was spin-coated (3000 rpm, 30 s) onto the gold substrates, which were then annealed for 10 min at 90°C on a hotplate. To release the transfer membrane, the substrates were floated on a gold etchant (Gold Etchant Standard, Sigma–Aldrich). After release, the membrane was transferred onto pure water multiple times for cleaning before being transferred onto the target substrate. After a final annealing step (80°C/150°C for 30 min each), the membrane was washed away with toluene [47].

IJD-MoS_2 films with nominal thicknesses of 30 and 120 nm, hereafter referred to as thin and thick films, respectively, were deposited using a laboratory-grade IJD system onto Pt/Si substrates (~240 nm Pt deposited by electron-beam evaporation). Prior to deposition, the substrates were solvent-cleaned by sonication in acetone and isopropanol (Sigma–Aldrich). A cylindrical MoS_2 target (Ø = 5 cm, thickness = 0.5 cm, purity 99.9%) was purchased from Testbourne Ltd. (Basingstoke, UK). The base pressure in the IJD chamber was 5×10^{-6} mbar and increased to 1×10^{-3} mbar during plasma formation, with argon used as the working gas. An acceleration voltage of 15 kV and a discharge frequency of 60 Hz were applied. Depositions were carried out at room temperature, yielding as-deposited samples. Subsequently, the as-deposited MoS_2 films were annealed under ultra-high vacuum (UHV) conditions ($p = 2 \times 10^{-9}$ mbar) at 250°C for 120 min. Briefly, in the IJD process an ionized Ar working gas passes through a convergent-divergent De Laval nozzle generating an ultrafast supersonic jet that enters a hollow cathode, where cascade ionization produces a high-density electron plasma; pulsed discharges ($f \leq 300$ Hz, pulse length 100–300 ns, $|V| \leq 30$ kV, $I^{peaN} \leq 6$ kA) direct this electron beam onto the rotating MoS_2 target, ablating molecular-sized Mo_xS_y species that condense on the rotating substrate. Further details on the IJD technique and deposition parameters are given in Refs [25, 27, 33].

Transmission electron microscopy (TEM). TEM lamellae of the IJD-MoS_2 thick film (both as-deposited and annealed states) were prepared by standard focused-ion-beam (FIB) lift-out. Bright-field TEM imaging was performed at 200 kV using a field-emission JEOL JEM-2200FS transmission electron microscope equipped with an in-column Omega energy filter at the IMEM-CNR institute (Parma, Italy). Samples for TEM were prepared by gently rubbing the MoS_2 thin film onto standard carbon-coated copper TEM grids. Bright-field images were collected to reveal contrast between amorphous and crystalline regions. Fast Fourier transform (FFT) analysis of selected image areas was used to identify hexagonal lattice periodicities and measure interplanar spacings, confirming assignment to the (002) and (100) planes of 2H-MoS_2.

XAS measurements were carried out at the BEAR beamline of CNR-IOM at Elettra [48, 49] in s-polarization conditions, with an impinging angle of 45° with respect to the sample normal. Absorption was collected in total electron yield mode by measuring the drain current from the sample holder with an applied repulsive voltage of −100 V. Resolution was 0.1–0.2 eV. The drain current was normalized to the impinging photon flux, as measured with a calibrated photodiode (IRD AXUV-100).

Acknowledgements

The authors would like to thank A. Pedrielli for TEM lamella preparation of IJD-MoS2 films and F. Rossi for supporting the TEM analysis.

Open access publishing facilitated by Universita degli Studi di Modena e Reggio Emilia, as part of the Wiley - CRUI-CARE agreement.

Funding

This research was funded by the Italian MUR under PRIN 2022 Project '2D-EMMA' (Project n. 202289PMBP, CUP: B53D23004010006), the under PRIN 2022 Project 'PETRA' (Project n. 2022T7ZSEK, CUP B53D23001860006), the under PNRR 2023 Project 'NQSTI' (Project n. PE0000023, CUP B53C22004180005) in the frame of Next Generation EU and by the European Commission under the HORIZON-MSCA-2023-PF-01 project CHIMERA, ID 101151367.

Conflicts of Interest

The authors declare no conflicts of interest.

Data Availability Statement

The data that support the findings of this study are available from the corresponding author upon reasonable request.

References

1. A. Splendiani, L. Sun, Y. Zhang, et al., "Emerging Photoluminescence in Monolayer MoS_2," *Nano Letters* 10 (2010): 1271–1275, https://doi.org/10.1021/nl903868w.

2. K. F. Mak, C. Lee, J. Hone, J. Shan, and T. F. Heinz, "Atomically Thin MoS_2: A New Direct-Gap Semiconductor," *Physical Review Letters* 105 (2010): 136805, https://doi.org/10.1103/PhysRevLett.105.136805.

3. A. Kuc, N. Zibouche, and T. Heine, "Influence Of Quantum Confinement On The Electronic Structure Of The Transition Metal Sulfide TS_2," *Physical Review B* 83 (2011): 245213, https://doi.org/10.1103/PhysRevB.83.245213.

4. J. H. Kim, H. Sung, and G. H. Lee, "Phase Engineering Of Two-Dimensional Transition Metal Dichalcogenides," *Small Science* 4 (2024): 2702.

5. K. S. Novoselov, D. Jiang, F. Schedin, et al., "Two-Dimensional Atomic Crystals," *Proceedings of the National Academy of Sciences* 102 (2005): 10451–10453, https://doi.org/10.1073/pnas.0502848102.

6. M. A. Lukowski, A. S. Daniel, F. Meng, A. Forticaux, L. Li, and S. Jin, "Enhanced Hydrogen Evolution Catalysis From Chemically Exfoliated Metallic MoS_2 Nanosheets," *Journal of the American Chemical Society* 135 (2013): 10274–10277, https://doi.org/10.1021/ja404523s.

7. T. F. Jaramillo, K. P. Jørgensen, J. Bonde, J. H. Nielsen, S. Horch, and I. Chorkendorff, "Identification of Active Edge Sites for Electrochemical H_2 Evolution From MoS_2 Nanocatalysts," *Science* 317 (2007): 100–102, https://doi.org/10.1126/science.1141483.

8. X. Zhang, Z. Zhang, S. Zhang, et al., "Graphene Quantum Dots Decorated TiO_2 Nanotube Arrays With Enhanced Photoelectrochemical Performance," *Nanoscale* 8 (2016): 13636.

9. T. Liu, C. Wang, X. Gu, et al., "Drug Delivery With PEGylated MoS_2 Nano-sheets for Combined Photothermal and Chemotherapy of Cancer," *Advanced Materials* 26 (2014): 3433–3440, https://doi.org/10.1002/adma.201305256.

10. J. N. Coleman, M. Lotya, A. O'Neill, et al., "Two-Dimensional Nanosheets Produced by Liquid Exfoliation of Layered Materials," *Science* 331 (2011): 568–571, https://doi.org/10.1126/science.1194975.

11. S. S. Chou, M. De, J. Kim, et al., "Ligand Conjugation of Chemically Exfoliated MoS_2," *Journal of the American Chemical Society* 135 (2013): 4584–4587, https://doi.org/10.1021/ja310929s.

12. Y.-H. Lee, X.-Q. Zhang, W. Zhang, et al., "Synthesis of Large-Area MoS_2 Atomic Layers With Chemical Vapor Deposition," *Advanced Materials* 24 (2012): 2320–2325, https://doi.org/10.1002/adma.201104798.

13. D. Dumcenco, D. Ovchinnikov, K. Marinov, et al., "Large-Area Epitaxial Monolayer MoS_2," *ACS Nano* 9 (2015): 4611–4620, https://doi.org/10.1021/acsnano.5b01281.

14. M.-H. Chiu, C. Zhang, H.-W. Shiu, et al., "Determination Of Band Alignment In The Single-Layer MoS_2/WSe_2 Heterojunction," *Nature Communications* 6 (2015): 7666, https://doi.org/10.1038/ncomms8666.

15. Y. R. Lim, W. Song, J. K. Han, et al., "Wafer-Scale, Homogeneous MoS_2 Layers on Plastic Substrates for Flexible Visible-Light Photodetectors," *Advanced Materials* 28 (2016): 5025–5030, https://doi.org/10.1002/adma.201600606.

16. A. S. George, Z. Mutlu, R. Ionescu, et al., "Wafer Scale Synthesis and High Resolution Structural Characterization of Atomically Thin MoS_2 Layers," *Advanced Functional Materials* 24 (2014): 7461–7466, https://doi.org/10.1002/adfm.201402519.

17. W. Zheng, T. Xie, Q. Yu, et al., "Patterned Growth of P-Type MoS_2 Atomic Layers Using Sol–Gel as Precursor," *Advanced Functional Materials* 26 (2016): 6371–6379, https://doi.org/10.1002/adfm.201602494.

18. M. V. Nardi, L. Giovanelli, A. Vegliante, et al., "Versatile and Scalable Strategy To Grow Sol–Gel Derived 2H-MoS_2 Thin Films With Superior Electronic Properties: A Memristive Case," *ACS Applied Materials & Interfaces* 10 (2018): 34392–34400, https://doi.org/10.1021/acsami.8b12596.

19. N. Mutz, M. Blum, S. K. Batabyal, et al., "Pulsed Thermal Deposition Of Binary And Ternary Transition Metal Dichalcogenide Monolayers And Heterostructures," *Applied Physics Letters* 114 (2019): 162101, https://doi.org/10.1063/1.5088758.

20. M. I. Serna, J. Woo, Y. Kim, S. Lee, M. Kim, and J. Lee, "Large-Area Deposition of MoS_2 by Pulsed Laser Deposition With In Situ Thickness Control," *ACS Nano* 10 (2016): 6054–6061, https://doi.org/10.1021/acsnano.6b01636.

21. F. Tumino, C. S. Casari, M. Passoni, V. Russo, and A. L. Bassi, "Pulsed Laser Deposition Of Single-Layer MoS_2 on Au(111): From Nanosized Crystals To Large-Area Films," *Nanoscale Advances* 1 (2019): 643–655, https://doi.org/10.1039/C8NA00126J.

22. S. Hussain, M. A. Shehzad, D. Vikraman, H.-S. Kim, J. Jung, and S.-J. Kim, "Large-Area, Continuous And High Electrical Performances Of Bilayer To Few Layers MoS_2 Fabricated by RF Sputtering Via Post-Deposition Annealing Method," *Scientific Reports* 6 (2016): 30791.

23. J. Tao, H. Chou, Y. Wu, H. Pan, and X. Xu, "Growth of Wafer-Scale MoS_2 Monolayer By Magnetron Sputtering," *Nanoscale* 7 (2015): 2497–2503, https://doi.org/10.1039/C4NR06411A.

24. G. Siegel, Y. P. Venkata Subbaiah, M. C. Prestgard, and A. Tiwari, "Growth Of Centimeter-Scale Atomically Thin MoS_2 Films By Pulsed Laser Deposition," *APL Materials* 3 (2015): 056103.

25. C. Tomasi Cebotari, C. Gatsios, A. Pedrielli, et al., "Optimizing Crystalline MoS_2 Growth on Technologically Relevant Platinum Substrates Using Ionized Jet Deposition: Interface Interactions and Structural Insights," *Surfaces* 8 (2025): 38, https://doi.org/10.3390/surfaces8020038.

26. E. Campedelli, M. Mazzucato, M. Parnigotto, et al., "Ionized Jet Deposition of MoS_2 on Gas Diffusion Layer Electrodes for Next Generation Alkaline Electrolyzers," *Advanced Sustainable Systems* 9 (2025): 2400979, https://doi.org/10.1002/adsu.202400979.

27. A. Ghiami, M. Timpel, A. Chiappini, M. V. Nardi, and R. Verucchi, "Synthesis of MoS_2 Thin Film by Ionized Jet Deposition: Role of Substrate and Working Parameters," *Surfaces* 3 (2020): 683–693, https://doi.org/10.3390/surfaces3040045.

28. J. Skocdopole, P. Nozar, M. Netopilik, and L. Kalvoda, "Preparation of Polymeric Coatings by Ionized Jet Deposition Method," *Acta Polytechnica CTU Proceedings* 9 (2017): 26–31.

29. A. Gambardella, M. Berni, A. Russo, and M. Bianchi, "A Comparative Study Of The Growth Dynamics Of Zirconia Thin Films Deposited By Ionized Jet Deposition Onto Different Substrates," *Surface and Coatings Technology* 337 (2018): 306–312, https://doi.org/10.1016/j.surfcoat.2018.01.026.

30. D. Menossi, S. Di Mare, I. Rimmaudo, et al., IEEE 44th Photovoltaic Specialists Conference (PVSC) (IEEE, 2017), 2372–2375.

31. J. Skočdopole, L. Kalvoda, P. Nozar, and M. Netopilík, "Preparation Of Polymeric Coatings By Ionized Jet Deposition Method," *Chemical Papers* 72 (2018): 1735–1739, https://doi.org/10.1007/s11696-018-0426-6.

32. A. Liguori, C. Gualandi, M. L. Focarete, F. Biscarini, and M. Bianchi, "The Pulsed Electron Deposition Technique For Biomedical Applications: A Review," *Coatings* 10 (2019): 16.

33. M. Timpel, G. Ligorio, A. Ghiami, et al., "2D-MoS_2 Goes 3D: Transferring Optoelectronic Properties of 2D MoS_2 To A Large-Area Thin Film," *npj 2D Materials and Applications* 5 (2021): 64, https://doi.org/10.1038/s41699-021-00244-x.

34. J. Stohr, "Springer Series In Surface Sciences," *NEXAFS Spectroscopy* (Springer, 1992).

35. G. Kamada, G. Venugopal, M. Kotsugi, T. Ohkochi, M. Suemitsu, and H. Fukidome, "Element- and Site-Specific Many-Body Interactions in Few-Layer MoS_2 During X-Ray Absorption Processes," *Physica Status Solidi (A) Applications and Materials Science* 216 (2019): 1800539.

36. M. Lee, Y. Kim, A. Y. Mohamed, et al., "Direct Evidence of Electronic Interaction at the Atomic-Layer-Deposited MoS_2 Monolayer/SiO_2

Interface," *ACS Applied Materials & Interfaces* 12 (2020): 53852–53859, https://doi.org/10.1021/acsami.0c17544.

37. A. Parija, Y. H. Choi, Z. Liu, et al., "Mapping Catalytically Relevant Edge Electronic States of MoS_2," *ACS Central Science* 4 (2018): 493–503, https://doi.org/10.1021/acscentsci.8b00042.

38. M. Krbal, J. Prikryl, V. Prokop, I. Pis, F. Bondino, and A. V. Kolobov, "Formation Of Oriented Layered MoS_2 From Amorphous Thin Film Revealed By Polarized X-Ray Absorption Spectroscopy," *Applied Physics Letters* 121 (2022): 192105, https://doi.org/10.1063/5.0106886.

39. M. Dai, B. Zhou, and D. Yan, "Rare Earth Single-Atomic Hybrid Glasses for Near-Infrared II Optical Waveguides," *Angewandte Chemie International Edition* 64 (2025): 202505322, https://doi.org/10.1002/anie.202505322.

40. P. Li, Z. Qi, and D. Yan, "Rare Earth Er-Nd Dual Single-Atomic Catalysts for Efficient Visible-light Induced CO_2 Reduction to C_nH_{2n+1} OH (n =1, 2)," *Angewandte Chemie International Edition* 63 (2024): 202411000, https://doi.org/10.1002/anie.202411000.

41. Y. Zhao, H. Hu, X. Yang, D. Yan, and Q. Dai, "Tunable Electronic Transport Properties of 2D Layered Double Hydroxide Crystalline Microsheets With Varied Chemical Compositions," *Small* 12 (2016): 4471–4476, https://doi.org/10.1002/smll.201601354.

42. Z. Guo, W. Ye, X. Fang, et al., "Amorphous Cobalt–Iron Hydroxides As High-Efficiency Oxygen-Evolution Catalysts Based On A Facile Electrospinning Process," *Inorganic Chemistry Frontiers* 6 (2019): 687–693, https://doi.org/10.1039/C8QI01320A.

43. W. Ye, M. Arif, X. Fang, M. A. Mushtaq, X. Chen, and D. Yan, "Efficient Photoelectrochemical Route for the Ambient Reduction of N_2 to NH_3 Based on Nanojunctions Assembled From MoS_2 Nanosheets and TiO_2," *ACS Applied Materials & Interfaces* 11 (2019): 28809–28817, https://doi.org/10.1021/acsami.9b06596.

44. X. Zhang, S. Wang, C. K. Lee, et al., "Unravelling The Effect Of Sulfur Vacancies On The Electronic Structure Of The MoS_2 Crystal," *Physical Chemistry Chemical Physics* 22 (2020): 21776–21783, https://doi.org/10.1039/C9CP07004D.

45. M. Heyl, D. Burmeister, T. Schultz, et al., "Thermally Activated Gold-Mediated Transition Metal Dichalcogenide Exfoliation and a Unique Gold-Mediated Transfer," *physica status solidi (RRL)—Rapid Research Letters* 14 (2020): 2000408, https://doi.org/10.1002/pssr.202000408.

46. G. Z. Magda, J. Petõ, G. Dobrik, C. Hwang, L. P. Biró, and L. Tapasztó, "Exfoliation Of Large-Area Transition Metal Chalcogenide Single Layers," *Scientific Reports* 5 (2015): 14714, https://doi.org/10.1038/srep14714.

47. A. Gurarslan, Y. Yu, L. Su, et al., "Surface-Energy-Assisted Perfect Transfer of Centimeter-Scale Monolayer and Few-Layer MoS_2 Films Onto Arbitrary Substrates," *ACS Nano* 8 (2014): 11522–11528, https://doi.org/10.1021/nn5057673.

48. S. Nannarone, F. Borgatti, A. DeLuisa, et al., "The BEAR Beamline at ELETTRA," *AIP Conference Proceedings* 705 (2004): 450, https://doi.org/10.1063/1.1757831.

49. L. Pasquali, A. DeLuisa, and S. Nannarone, "The UHV Experimental Chamber for Optical Measurements (Reflectivity and Absorption) and Angle Resolved Photoemission of the BEAR Beamline at ELETTRA," *AIP Conference Proceedings* 705 (2004): 1142.